JOURNAL OF AIRCRAFT
Vol. 35, No. 1, January–February 1998

New Adaptive Wall Test Section for Three-Dimensional Wind-Tunnel Testing

Byeong-Hee Chang* and Bongzoo Sung†
Korea Aerospace Research Institute, Taejon 305-333, Republic of Korea
and
Keun-Shik Chang‡
Korea Advanced Institute of Science and Technology, Taejon 305-701, Republic of Korea

The flexible wall contour of the new adaptive wall test section is represented as a combination of base streamlines. The combination coefficients are optimized to minimize the wall interference that is taken as the summation of the area weighted surface pressure difference between the free air and test section results. The numerical simulations show that the new adaptive wall test section produces similar results to the free air results. This new algorithm is free from the deficiencies of conventional algorithms such as the dependence on a target line, a pressure hole distribution, and influence coefficients. This new adaptation algorithm may be applied to real tests in which conventional adaptation algorithms fail.

Nomenclature

B = wing semispan
C = wing root chord
dA = cell area on the reference surface or effective area of the pressure hole
H = test section's half-height
M = Mach number
W = test section width
x, y, z = Cartesian coordinates
Z = wall position in z coordinate
α = angle of attack or design variable
δ^* = displacement thickness of boundary layer

Subscripts
i, j = grid index or pressure hole index
∞ = freestream

Introduction

THE idea of the flexible adaptive wall test section (AWTS) has many benefits over the conventional ventilated wall test section. The adaptation algorithm and mechanism of AWTS for two-dimensional testing have been well established and verified through various tests.[1] The concept of the adaptation algorithm for two-dimensional testing is adapting the wall contours to match the inner real flow with the outer imaginary flow on the matching boundary. The adapted contours are equal to the free air streamlines compensated for the wall boundary layer.

On the analogy of a two-dimensional case, the ideal AWTS for three-dimensional testing should be adapted to a free air streamtube compensated for the wall boundary layer. In this respect, several concepts of three-dimensional AWTS such as the rubber tube,[2] the octagonal AWTS,[3] and the multislat AWTS[4] have been investigated. Nevertheless, they have weaknesses in practical use because of the complexity of hardware and software. Another method of three-dimensional adaptation, the segmented plenum chamber,[5] also has a restriction in its adaptation ability.[6] So far, it is concluded that the full three-dimensional streamtube adaptation is impractical and that the AWTS with two flexible walls is adequate for three-dimensional testing.[7] This means that if the top and bottom walls are contoured properly, the two-dimensional AWTS is successful for three-dimensional wind-tunnel testing.

Until now, several adaptation algorithms of two-dimensional AWTS for three-dimensional testing have been developed and tested. The first one[8] put a target line at the streamwise centerline, and the top and bottom walls were adapted to reduce wall interference on the target line. In a later research,[9] the target line was widened from the streamwise centerline to a streamwise line at any position. In these adaptation algorithms, the spanwise variation of the upwash interference is not considered and a wall-induced twist of the wing is produced. To reduce this spanwise variation, a swept target line[10] has been studied and proved to be effective to reduce the wall-induced twist. In these algorithms, adaptation displacements are calculated by the influence coefficients that are derived from the internal flow analysis like a linearized potential flow.

In spite of many advantages of these conventional adaptation algorithms, they have some deficiencies in general testing. The best location and shape of the target line for different model configurations is still unknown.[6] The proper distribution of the pressure hole is critical to the success of these adaptation algorithms.[6] Even though the theoretically derived influence coefficients are close to the measured ones,[11] a significant error may arise in some complex flows in which the theory of influence coefficients fails. Therefore, the adaptation algorithms based on the influence coefficients are not adequate to obtain the best wall contours in those complex flows.

In this study, a new adaptation algorithm of the two-dimensional AWTS for three-dimensional testing is suggested to overcome these deficiencies of the conventional algorithms. The flexible wall contours are obtained from the combination of base streamlines that can represent the flow characteristics around the model in the free air. The combination coefficients are determined by the optimization to minimize the wall interference. The performance of this algorithm is verified through numerical simulations. The effects of the base stream-

Received Dec. 15, 1996; revision received July 25, 1997; accepted for publication July 28, 1997.

*Senior Researcher, Aerodynamics Department, 52 Oun-dong, Yusung-gu. Member AIAA.
†Head, Aerodynamics Department, 52 Oun-dong, Yusung-gu. Member AIAA.
‡Professor, Department of Aerospace Engineering, 52 Kusung-dong, Yusung-gu. Member AIAA.

line selection and pressure hole distribution are also considered.

Numerical Analysis

Governing Equations and Numerical Method

In this study, the test section inner flow as well as the free airflow is computed numerically. The final wall shape of this new AWTS is determined by iterations, and a numerical simulation of the inner flow is necessary at each step. For this reason, the three-dimensional Euler equations are taken as the governing equations to save the computing time. The viscous effects including the boundary layers on the test section walls are discussed in the Application to Real Tests section.

The spatial differencing of the governing equations is based on the finite volume formulation. The flux vectors are differenced by the flux difference split (FDS) with Roe's approximate Riemann solver. The state variables on the cell interfaces are determined from the upwind-biased interpolation that needs the minmod limiter to maintain the monotonicity.

Time advancing is achieved by the implicit time integration with the spatially split approximate factorization and the diagonalization. Convergence of the steady solution is accelerated by the local time step.

The far-field boundary condition is computed from the characteristic theory, and the pressure on the solid wall is obtained from the normal momentum equation.

Test Section Configuration and Grid System

The size of test section is chosen to provide a 1% blockage ratio that is the limit in the conventional transonic ventilated wall test section. The test section height is 75% of the test section width. The configuration and the notation are shown in Fig. 1 in which B/W is 0.5395 and H/C is 1.0136.

To calculate the test section flow and the free airflow, the grid system is composed of three blocks. A single $C-H$ mesh wraps the wing and two $H-H$ meshes fill the exterior of the $C-H$ mesh (Fig. 1). The grid point connection on the block interfaces is done by a one-to-one connection that dispenses with time-consuming interpolation.

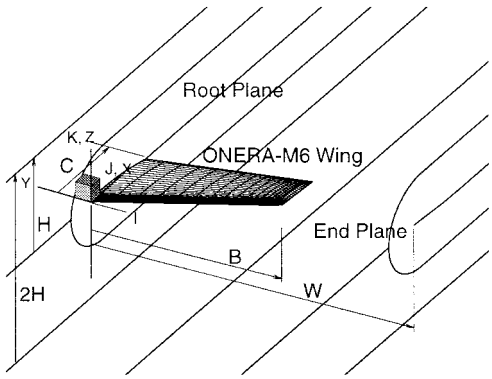

Fig. 1 Notation of test section and grid system.

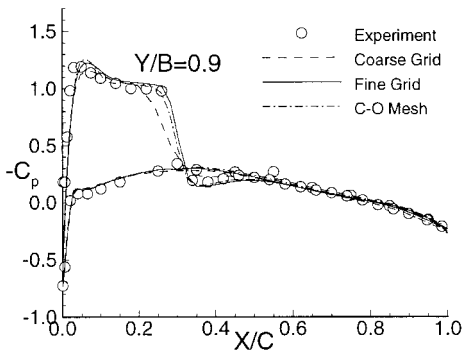

Fig. 2 Evaluation of the computation code on different grid systems at $M_\infty = 0.84$, $\alpha = 3.06$ deg.

Validation of Numerical Method

As a wing model, the ONERA M6 wing is selected to validate the computation code and the grid system. Figure 2 shows the comparison of the surface pressure distributions on the wing section in the free air. The computed results with the three-block system ($C-H$: 33 × 161 × 17, $H-H$: 33 × 97 × 33) and a single $C-O$ mesh ($C-O$: 121 × 35 × 49) agree well with the experimental results.[12] Despite some errors in severe flow gradient regions such as the leading edge and the shock, a reasonable result can be obtained with the coarse grid system ($C-H$: 27 × 97 × 17, $H-H$: 27 × 65 × 17). Hence, in this study, the coarse grid system is employed to save computing time in the optimizing process.

New Adaptation Algorithm

Adaptive Wall Model

The adaptation algorithms of two-dimensonal AWTS for three-dimensional testing intend not to eliminate but to reduce the wall interference, because this type of AWTS cannot be fully adapted to a streamtube shape. The purpose of the adaptation algorithms is set on finding the wall contours that minimize the wall interference. This minimum interference contour could be assumed to be similar to the geometrical mean streamline. Nevertheless, there is no evidence that the wall adaptation to the mean streamline can minimize the wall interference. A more elaborate wall adaptation algorithm is necessary and might be achieved by analyzing the flow structure in the free air.

Figure 3 shows the computed streamlines projected on the $x-z$ plane. The streamlines around the wing in the free air can be grouped into two patterns such as a washdown and a washup as a result of the wing tip vortex. If we assume that these streamlines around the wing belong to the two-dimensional linear vector space, there exist two linearly independent

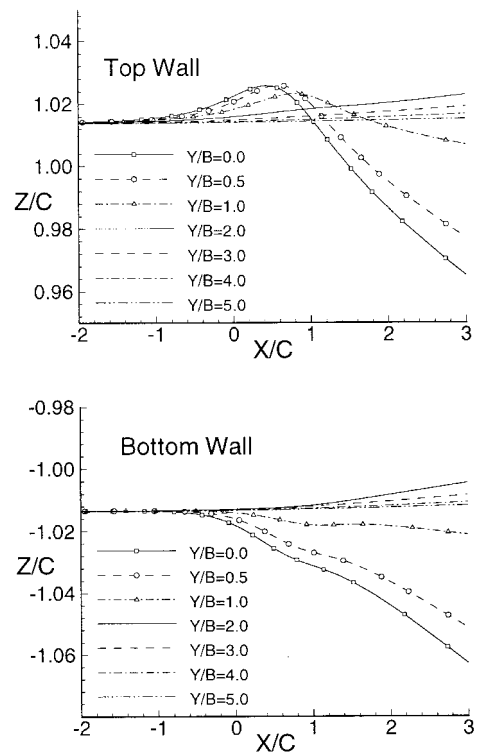

Fig. 3 Streamlines around the wing in the free air projected on $x-z$ plane at $M_\infty = 0.84$, $\alpha = 3.06$ deg.

streamlines, called base streamlines, which can represent any other streamline with a proper combination as

$$Z(x) = Z_w + \alpha_1[Z_1(x) - Z_w] + \alpha_2[Z_2(x) - Z_w] \qquad (1)$$

where Z_w is fixed as the unadapted flat wall position, $Z_1(x)$ and $Z_2(x)$ are base streamlines, and α_1 and α_2 are combination coefficients.

The base streamline should be selected from each flow pattern, but there are no rigorous criteria for which streamline should be chosen. This dilemma can be settled if we can prove that this algorithm is not sensitive to the selection of base streamlines.

For this reason we first compute a wing in the half-free air that has side walls only, and the streamlines on the root plane and the opposite wall plane (end plane) are taken as $Z_1(x)$ and $Z_2(x)$, respectively. And later we prove that a different set of base streamlines produces a similar residual interference.

The minimum interference wall contour among the contours determined by Eq. (1) can be obtained by the optimum choice of the combination coefficients. Therefore, α_1 and α_2 should be determined through the optimization procedure that minimizes the wall interference.

Optimization

In the given test condition and the model configuration, the wall interference of the two-dimensional AWTS is dependent on the wall shape only. It means that the wall interference of the two-dimensional AWTS contoured by Eq. (1) is a function of α_1 and α_2, which are the design variables in optimization. The objective function that is a target of the optimization naturally becomes the wall interference. To exclude the pressure hole dependency, the wall interference can be represented by the summation of the area weighted surface pressure difference between the free air result and the test section results, namely,

$$\varepsilon = f(\alpha_1, \alpha_2) = \sum_{ij} |\Delta p_{ij}(\alpha_1, \alpha_2)| \, dA_{ij} \qquad (2)$$

$$\Delta p_{ij} = p_{TS}(i, j) - p_{Free}(i, j) \qquad (3)$$

where p_{Free} and p_{TS} are pressure on the reference surface in the free air result and in the test section result, respectively. In this study, the model surface is taken as the reference surface to save computing time; because p_{Free} is computed from the free air once, it is not necessary to be updated during the optimization procedure.

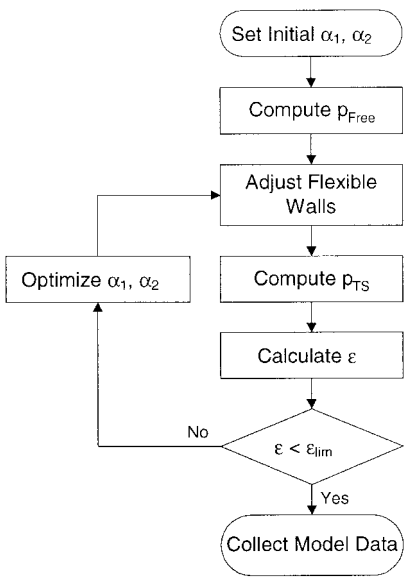

Fig. 4 Schematic diagram of the new adaptation algorithm for numerical verification.

The adaptive wall model represented by Eq. (1) is optimized with the two-variable optimization that is composed of searching the optimum directional vector and finding the optimum point along the determined direction. In this study, the conjugate direction method developed by Fletcher and Reeves[13] is used to search the optimum direction. This method is not the most powerful one, but it is very easily incorporated into the computation code and requires very little computer storage. To find the optimum point along the determined direction, the finding bounds algorithm, the golden section method, and the quadratic polynomial approximation are applied successively.[14] If we assume that the optimum point lies on the line, $\alpha_2 = 1 - \alpha_1$, the one-variable optimization is enough and we can save computing time.

Figure 4 shows the schematic diagram of the new adaptation algorithm simplified for numerical verification in this study. The optimization procedure is continued until ε is less than an allowable interference ε_{lim}. To apply it to real tests, we have to make some changes, which are discussed later.

Results and Discussion

Figure 5 shows the convergence of the one-variable optimization. After finding the bounds of the minimum point, the golden section method narrows down the bounds. After a few steps of the golden section method, the final solution is obtained from the quadratic polynomial approximation. This procedure reduces the wall interference ε to 32.4% of the flat wall result ε_0, but it is still less than satisfactory.

Figure 6 shows the distribution of the relative wall interference $\varepsilon/\varepsilon_0$ plotted on the $\alpha_1 - \alpha_2$ plane. The one-variable optimization assumption means that the minimum interference point is searched along the line, $\alpha_2 = 1 - \alpha_1$. But, as shown in Fig. 6, the minimum interference point is not located on this line. To find this minimum interference point, a two-variable optimization is necessary. The wall interference is in-

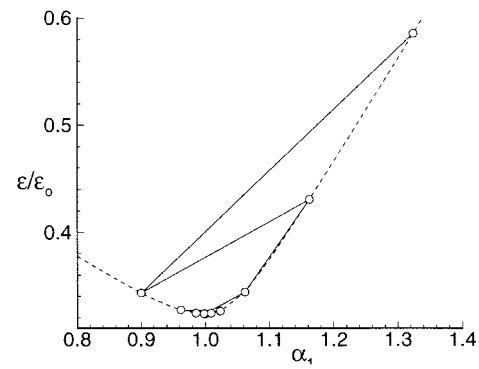

Fig. 5 Convergence of one-variable optimization at $M_\infty = 0.8$, $\alpha = 3.06$ deg.

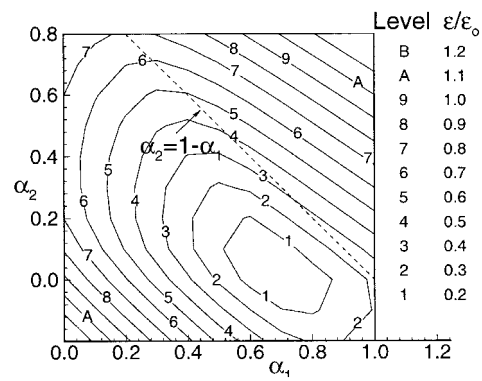

Fig. 6 Distribution of the objective function ($\varepsilon/\varepsilon_0$) on α_1–α_2 plane at $M_\infty = 0.8$, $\alpha = 3.06$ deg.

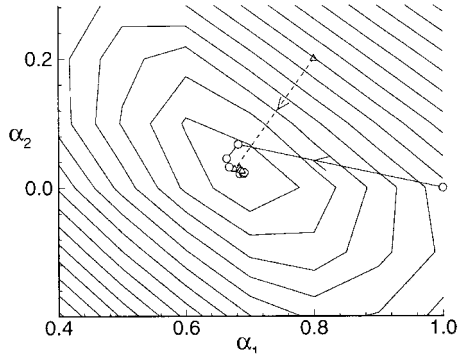

Fig. 7 Trajectories of the two-variable optimization at $M_\infty = 0.8$, $\alpha = 3.06$ deg.

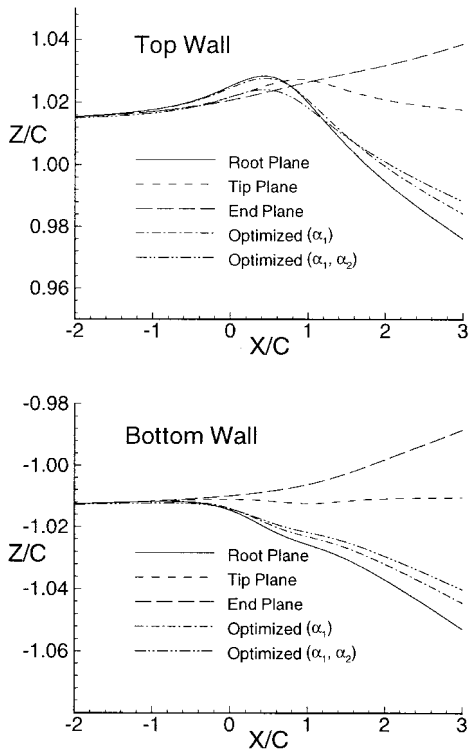

Fig. 8 Comparison of the optimized wall contours with base streamlines at $M_\infty = 0.8$, $\alpha = 3.06$ deg.

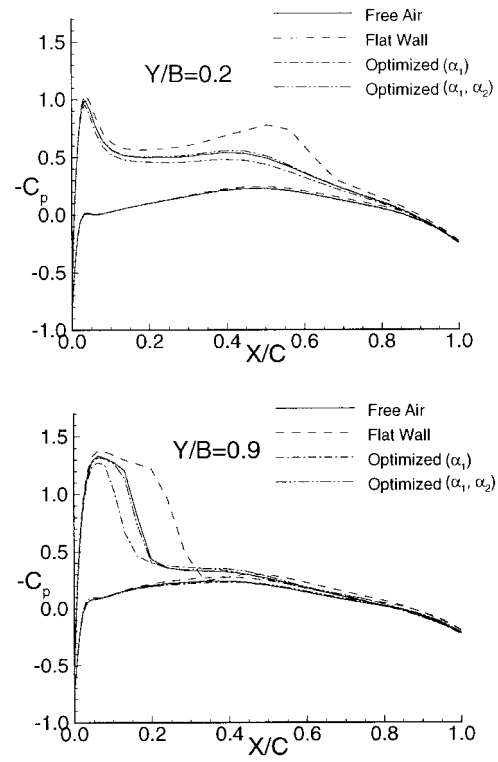

Fig. 9 Wall interference reduction on the surface pressure distribution at $M_\infty = 0.8$, $\alpha = 3.06$ deg.

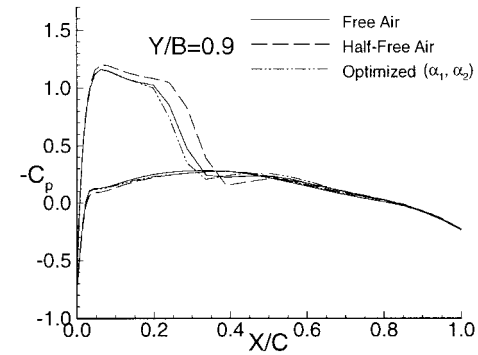

Fig. 10 Wall interference reduction on surface pressure distribution at $M_\infty = 0.84$, $\alpha = 3.06$ deg.

creased monotonically from the minimum point and no local minimum exists. This fact guarantees the success of a two-variable optimization. As described previously, the conjugate direction method is used for finding the optimum direction.

Figure 7 shows the trajectories of the two-variable optimization started from different initial states. Both of them are converged to the same minimum interference point via different paths. This means that the optimum wall shape of two-dimensional AWTS for three-dimensional testing can be obtained by the two-variable optimization procedure, even though its convergence rate depends on the initial wall shape.

The flexible wall contours obtained by the two-variable optimization are slightly different from the ones by the one-variable optimization as shown in Fig. 8. The top and bottom walls of the two-dimensional AWTS for three-dimensional testing have single curvatures as the optimized contours.

Performance of the New Adaptation Algorithm

In Fig. 9, the performance of the new two-dimensional AWTS is presented in aspect of the surface pressure distribution on the wing section. There is severe discrepancy between the free air result and the unadapted wall (flat wall) result. Because of the blockage effect, the flow around the model is accelerated. Hence, the supersonic region on the model is enlarged and the shock position shifts downward. This discrepancy is reduced by the one-variable optimization, but it is still high. Further reduction can be done by the two-variable optimization. The result of the two-dimensional AWTS adapted by the two-variable optimization is very close to the free air result.

As the Mach number increases to $M_\infty = 0.84$, the shock moves further downward. In the flat wall test section, the shock reaches the trailing edge and no solution is obtained (Fig. 10). This means that the flow Mach number, $M_\infty = 0.84$, is over the choking Mach number of the flat wall test section. But the two-dimensional AWTS adapted by the two-variable optimization is able to avoid the choke state and give a very close solution to the free air result. Moreover, its result is better than the result of the half-free air in which the base streamlines are obtained. In the half-free air, there are no top and bottom walls and the wall interference is generated from the sidewalls only. The performance of the new two-dimensional AWTS model is very promising.

Sensitivity to the Base Streamline Selection

To be utilized as a practical tool, it should be proven that the new adaptation algorithm performance is not sensitive to

the selection of the base streamlines. In the real wind-tunnel test, there is no way to find out the streamlines in the half-free air. These streamlines can only be obtained by a computational fluid dynamics (CFD) method that inherently brings a numerical error. Moreover, there is no evidence that the best positions for the base streamlines are on the end plane and the root plane. The effect of these two errors, a CFD error and a position error, is negligible if the different selection of base streamlines produces the same result. To verify this fact, a different set of the base streamlines is taken at midspan ($Y = 0.29W$) and midpoint ($Y = 0.78W$) between the wing tip and the end plane. Their shapes are compared with the original base streamlines (Fig. 11).

In Fig. 12, the wall interference of the unoptimized ($N = 0$) two-dimensional AWTS, in which α_1 is 1.0 and α_2 is 0.0, depends on the selection of the base streamlines. N is the number of the directional search that means the trajectory segment in Fig. 7. After the first directional search is completed ($N = 1$), the difference nearly disappears. Though its convergence rate is dependent on the initial state, it usually converges after several direction changes.

The effect of the base streamline selection is compared with respect to the pressure distribution (Fig. 13). The result of the new streamlines is slightly worse than that of the previous ones, but it is still close to the free air result. From this result, we can conclude that the base streamlines of the new two-dimensional AWTS can be taken from the CFD result, and its numerical error and position error cause no significant effect on the optimized result.

Pressure-Hole Dependency

This new adaptation algorithm assesses the interference without a target line and calculates its adaptation displacement with the design variables in Eq. (1) instead of the influence coefficients. Among the deficiencies of the conventional adaptation algorithms, the pressure-hole dependency remains to be solved. In this study, the test section flow is simulated by the numerical code. The pressure-hole distribution in real tests can be considered as the surface grid distribution in this study. For this reason, different surface grids are generated (Fig. 14). The tip-clustered mesh is the old one that has been applied so far, and the biclustered mesh is a new one. The three-dimensional grid is generated by layering two-dimensional $x-z$ grid along the y direction. Hence, the grid distribution on the test section wall is same as that on the wing surface.

To verify the pressure-hole independency of the new adaptation algorithm, we have to prove that the optimized result with the new mesh is equal to that with the old mesh. Figure 15 shows that this requirement has been fulfilled. Both results agree well with each other, even though there is a slight discrepancy between the two. This slight discrepancy may be caused by the numerical error of computation code itself instead of from the new adaptation algorithm. To clarify this fact, it is necessary to examine the grid dependency of the computation code itself.

Figure 16 shows the free air results on the two meshes compared in Fig. 14. There is an amount of discrepancy similar to the optimized test section results (Fig. 15). The discrepant patterns are also similar. If we double the spanwise grid density as shown in Fig. 17, the discrepancy in the free air results between the tip-clustered grid and the biclustered grid nearly disappears (Fig. 18).

Any CFD code requires the minimum grid density to secure the grid independency. Under this grid density, its computation results are dependent on the grid distribution. Therefore, the slight discrepancy in Fig. 15 seems to be a result of the CFD code itself and not of the adaptation algorithm. In other words, if the pressure-hole density is sufficient or measured pressures are interpolated well, this new adaptation algorithm is independent of the pressure-hole distribution.

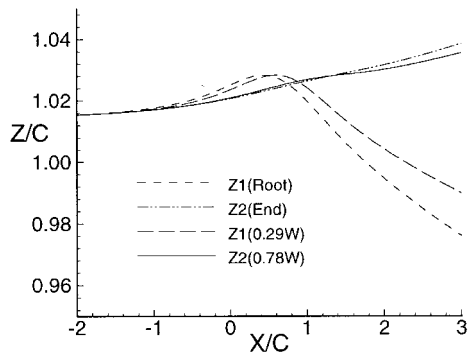

Fig. 11 Comparison of the different set of base streamlines at $M_\infty = 0.8$, $\alpha = 3.06$ deg.

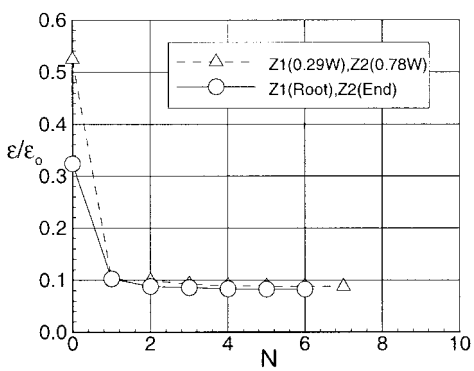

Fig. 12 Convergence comparison of the different sets of base streamlines at $M_\infty = 0.8$, $\alpha = 3.06$ deg.

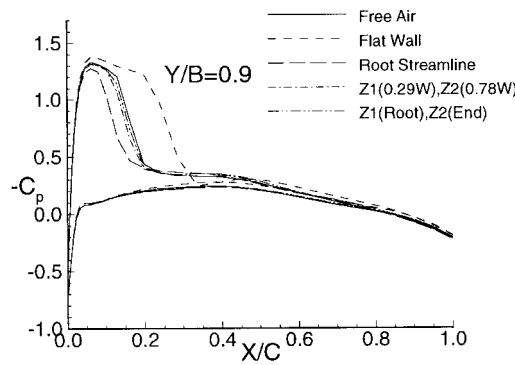

Fig. 13 Base streamline effect on reducing wall interference at $M_\infty = 0.8$, $\alpha = 3.06$ deg.

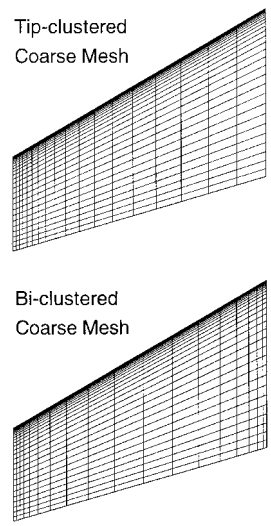

Fig. 14 Comparison of two different coarse meshes on the wing surface.

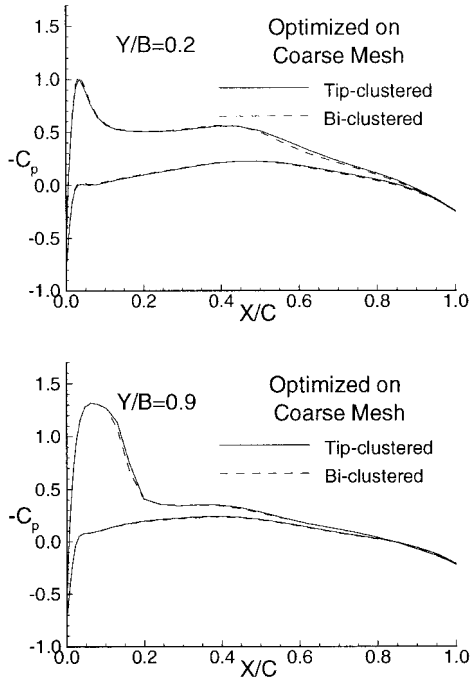

Fig. 15 Grid distribution effect on the optimized results at M_∞ = 0.8, α = 3.06 deg.

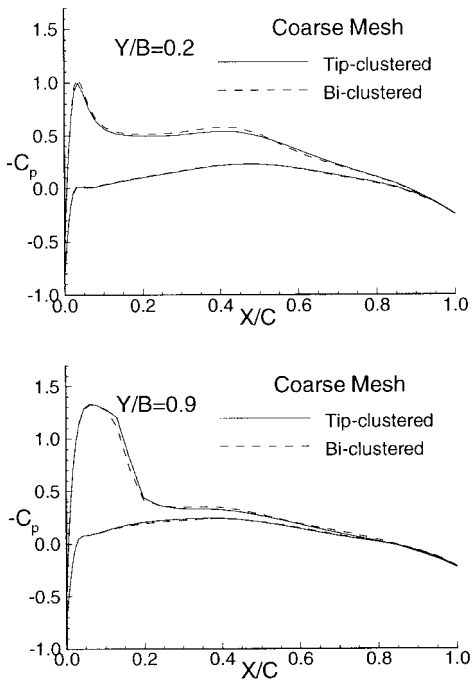

Fig. 16 Grid distribution effect on the free air results with coarse meshes at M_∞ = 0.8, α = 3.06 deg.

Application to Real Tests

Even though the new two-dimensional AWTS for three-dimensional testing has proved to be successful and free from the deficiencies of conventional adaptation algorithms, there remain some considerations to be applied to real tests. In this study, p_{Free} in Eq. (2) is taken as the computed pressure on the model surface, but it is not achievable in real tests. If any CFD code can compute the pressure on the model surface with sufficient accuracy, then wind-tunnel tests are unnecessary. Even the most elaborate CFD code still has some deficiencies in accuracy, computing cost, and reliability for computing some complex flows. If we assume a simple flow like the outer imaginary flow of test section walls, an accurate computational result is obtainable, even through a simple integral method.

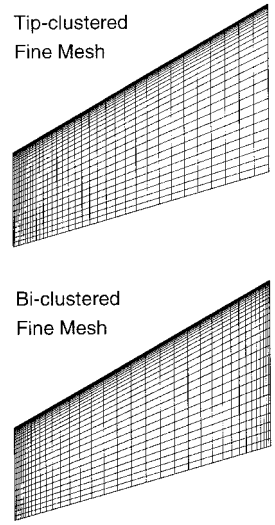

Fig. 17 Comparison of two different fine meshes on the wing surface.

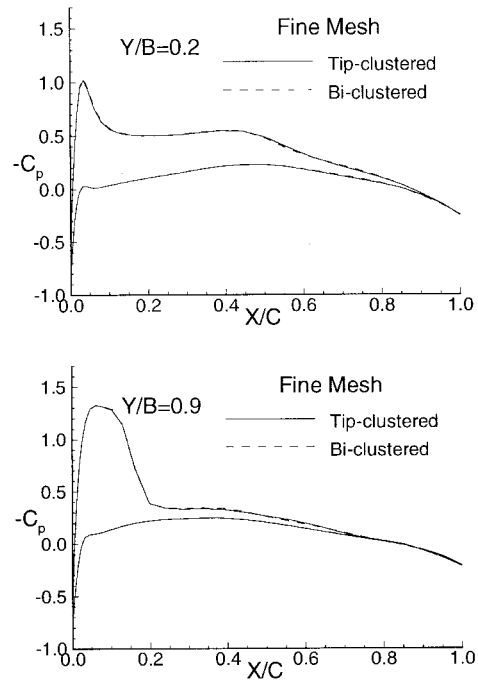

Fig. 18 Grid distribution effect on the free air results with fine meshes at M_∞ = 0.8, α = 3.06 deg.

For this reason, the reference surface in real tests is set to be the test section wall similar to the matching line in two-dimensional testing. In this case, p_{Free} and p_{TS} are regarded as the wall pressures computed from the outer imaginary flow and measured from the inner real flow, respectively. p_{Free} should be computed at every adaptation step, unlike this study, but computing time is not severe because a simple method like the integral method is taken to compute the outer imaginary flow.

In tests for any model producing more than two flow patterns, two base streamlines are not sufficient to represent all of the streamlines. The two-dimensional AWTS contoured by Eq. (1) with the two-variable optimization may not reduce the wall interference sufficiently. This situation can be improved by increasing the number of base streamlines to a quantity sufficient to represent all of the streamlines. The design variables should also be increased in proportion to the number of the base streamlines.

Although viscosity effect is ignored in this study to save computing time, the effective cross-sectional area in the real tests narrows down by δ^*. For this reason, even if the wall contour of AWTS is adapted to a free air streamtube, the wall pressure computed from the outer imaginary flow is not equal to the one measured from the inner testing flow. In the adaptation algorithm for two-dimensional testing, the effective aerodynamic wall contour, the geometrical wall contour compensated for δ^* on the inner wall, is used as the boundary of the outer imaginary flowfield.[15] This concept can be applied to the new adaptation algorithm. The effective aerodynamic wall contours can be obtained by compensating the geometrical wall contours for δ^* on the sidewalls as well as those on the top and bottom walls.

As a result, with some changes in Fig. 4, the new adaptation algorithm can be applied to the real tests. The step of Compute p_{Free} should be moved into the iteration loop, and the free air is replaced by the outer imaginary flow. The step of Compute p_{TS} is changed to Measure p_{TS}, and the reference surface is set on the flexible wall instead of the model surface. This new adaptation algorithm is similar to the conventional adaptation algorithm for two-dimensional testing,[15] except that the wall adjustment is done by the optimization instead of influence coefficients.

Conclusions

A new adaptation algorithm of two-dimensional AWTS for three-dimensional testing is suggested and verified through numerical simulations. This adaptation algorithm uses a two-variable optimization and finds out the optimum shape independent of the initial state. From the numerical simulations, it is verified that this adaptation algorithm works well in reducing the wall interference and is not sensitive to the base streamline selection. The base streamlines can be obtained by a CFD code with an allowable accuracy. The dependency of the pressure-hole distribution is not severe because the summation of the area weighted surface pressure interference is taken as the objection function. Therefore, the deficiencies of the conventional adaptation algorithm can be avoided in this new adaptation algorithm.

This algorithm may require more adapting and computing time than the conventional algorithms. But this algorithm can be applied safely for the case in which the conventional algorithms fail because of their own deficiencies.

References

[1]Wolf, S. W. D., "Wall Adjustment Strategy Software for Use with NASA Langley 0.3-Meter Transonic Cryogenic Tunnel Adaptive Wall Test Section," NASA CR-181694, Nov. 1988.

[2]Heddergott, A., and Wedemeyer, E., "Deformable Adaptive Wall Test Section for Three-Dimensional Wind Tunnel Testing," *Proceedings of the 14th International Council of the Aeronautical Sciences*, Vol. 1, International Council of the Aeronautical Sciences, Toulouse, France, 1984, pp. 66–75.

[3]Ganzer, U., Igeta, Y., and Ziemann, J., "Design and Operation of TU-Berlin Wind Tunnel with Adaptable Walls," *Proceedings of the 14th International Council of the Aeronautical Sciences*, Vol. 1, International Council of the Aeronautical Sciences, Toulouse, France, 1984, pp. 52–65.

[4]Starr, R. F., and Varner, M. O., "Application of the Adaptive Wall to High-Lift Subsonic Aerodynamic Testing — An Engineering Evaluation," *Proceedings of the AIAA 13th Aerodynamic Testing Conference*, AIAA, New York, 1984, pp. 284–291.

[5]Satyanarayana, B., Schairer, E., and Davis, S., "Adaptive-Wall Wind-Tunnel Development for Transonic Testing," *Journal of Aircraft,* Vol. 18, No. 4, 1981, pp. 273–279.

[6]Wolf, S. W. D, "Adaptive Wall Technology for Improved Wind Tunnel Testing Technology Techniques — A Review," *Progress Aerospace Sciences*, Vol. 31, No. 2, 1995, pp. 85–136.

[7]Harney, D. J., "Three-Dimensional Testing in a Flexible-Wall Wind Tunnel," *Proceedings of the AIAA 13th Aerodynamic Testing Conference*, AIAA, New York, 1984, pp. 276–283.

[8]Wedemeyer, E., "Wind Tunnel Testing of Three-Dimensional Models in Wind Tunnels with Two Adaptive Walls," Von Kármán Inst., TN-147, Oct. 1982.

[9]Rebstock, R., and Lee, E. E., "Capabilities of Wind Tunnels with Two Adaptive Walls to Minimize Boundary in 3-D Model Testing," *Proceedings of the NASA Langley Transonic Symposium*, Vol. 1, Pt. 2, 1988, pp. 891–910.

[10]Lewis, M. C., Taylor, N. J., and Goodyer, M. J., "Adaptive Wall Technology for Three-Dimensional Models at High Subsonic Speeds and Aerofoil Testing Through the Speed of Sound," *Proceedings of the European Forum on Wind Tunnels and Wind Tunnel Testing Techniques*, Royal Aeronautical Society, Southampton, England, UK, Sept. 1992, pp. 42.1–42.12.

[11]Neal, G., "The Experimental Verification of Wall Movement Influence Coefficients for an Adaptive Walled Test Section," NASA CR-181681, July 1988.

[12]Schmitt, V., and Charpin, F., "Pressure Distributions on The ONERA-M6-Wing at Transonic Mach Numbers," *Experimental Data Base for Computer Program Assessment*, Rept. of the Fluid Dynamics Panel Working Group 04, AGARD-AR-138, May 1979, B1-1–B1-44.

[13]Fletcher, R., and Reeves, C. M., "Function Minimization by Conjugate Gradients," *Computer Journal*, Vol. 7, No. 2, 1964, pp. 149–154.

[14]Vanderplaats, G. N., "Functions of One Variable," *Numerical Optimization Techniques for Engineering Design with Applications*, McGraw–Hill, New York, 1984, pp. 24–70.

[15]Lewis, M. C., "Aerofoil Testing in a Self-Streamlining Flexible Walled Wind Tunnel," NASA CR-4128, May 1988.